Adaptive Space-Time Equalization with Spatial Oversampling for Misaligned LoS MIMO

Lalitha Giridhar, Maryam Eslami Rasekh, Ahmet Dundar Sezer, Upamanyu Madhow
Department of Electrical and Computer Engineering
University of California, Santa Barbara
Santa Barbara, California 93106
{lalitha, rasekh, adsezer, madhow}@ucsb.edu

***Abstract*—Line-of-sight (LoS) millimeter wave (mmWave) multiple-input multiple-output (MIMO) is a promising approach for providing the ultra-high speed point to point links required for wireless backhaul in picocellular networks. The combination of large bandwidth and spatial multiplexing can sustain $100+$ Gbps links over 10s to 100s of meters, while the antenna form factors required for providing the necessary spatial degrees of freedom remain small due to the small carrier wavelength. However, the large bandwidth makes the system susceptible to geometric misalignments: relatively small misalignments can cause multi-symbol delay spread across the receiver aperture. Furthermore, as the signaling bandwidth approaches the limits of hardware (i.e., analog-to-digital converter (ADC)) capabilities, the *temporal oversampling* typically used to overcome intersymbol interference becomes infeasible. In this paper, we investigate an architecture for joint space-time equalization with *spatial oversampling* by introducing additional receive antennas while maintaining symbol-rate sampling. We consider linear space-time equalization, controlling complexity by employing an adaptive time window at each receiver. We illustrate tradeoffs between the size of the adaptive window and the spatial oversampling factor via analysis and simulation for a 4-stream, 128 Gbps, 100 m LoS link at 130 GHz with both horizontal and vertical misalignment of the 2D planar arrays. For example, we show, via a signal space analysis accompanied by simulation results, that error floors can be avoided via 2X spatial oversampling and a temporal window of 5.**

***Index Terms*—mmWave, LoS MIMO, space-time equalisation, adaptive, spatial oversampling, interference vectors, LMMSE signal recovery**

I. Introduction

Millimeter wave (mmWave) Line-of-Sight (LoS) multiple-input multiple-output (MIMO) communication systems have attracted rising interest due to their potential for offering high data rates comparable to those of optical links [1], [2]. For an LoS MIMO link, with a horizontal distance, or range, R between two-dimensional (2D) transmit and receive arrays having areas of A_T and A_R, respectively, the number of available spatial degrees of freedom (DoF), specified by [3], [4]

$$DoF_{\text{2D}} \approx \frac{A_T A_R}{R^2 \lambda^2} + 1 \tag{1}$$

This work was supported in part by ComSenTer, one of six centers in JUMP, a Semiconductor Research Corporation (SRC) program sponsored by DARPA.

scales inversely with the square of carrier wavelength λ, implying that the scaling with the carrier frequency $f_c = c/\lambda$ is quadratic, where c is the speed of light. In addition, transmission bandwidth typically scales linearly with carrier frequency; therefore, the overall data rates offered by an LoS MIMO link can potentially scale cubically with carrier frequency. This attractive scaling with increase in carrier frequency motivates exploration of LoS MIMO for mmWave and THz frequency bands.

Consider a 4×4 LoS MIMO system with a link distance of $100\,\text{m}$. At a carrier frequency of $130\,\text{GHz}$, the inter-antenna spacing required for a well-conditioned spatial channel is $34\,\text{cm}$. Therefore, with $20\,\text{GHz}$ bandwidth and Quadrature Phase Shift Keying (QPSK) modulation, $100+$ Gbps data rates (even after accounting for excess bandwidth and lightweight channel coding) can be achieved by such architectures with transmit and receive antenna sizes as small as $0.12\,m^2$. These relatively compact form factors, which can be shrunk further by continuing to increase the carrier frequency, open up the potential for opportunistic deployment (e.g., on lampposts) for relatively short-range wireless backhaul links. However, such LoS MIMO systems are prone to channel dispersion caused by small geometric misalignments [5]. At $20\,\text{GHz}$ sampling rate, even a small vertical misalignment (i.e., tilt) angle of 7.5° degrees at both transmit and receive arrays causes a 6 symbol channel delay spread, which results in a finite impulse response (FIR) space-time channel rather than the ideal spatial channel.

In principle, the frequency selectivity caused by geometric misalignments can be mitigated by employing conventional approaches such as frequency domain equalization [6], OFDM, and fractionally spaced equalization [7]. The increased dynamic range required for OFDM is a challenge for mmWave RF hardware design at both the transmitter and receiver. The temporal oversampling required for fractionally spaced equalization is also unattractive, given the challenge of analog-to-digital conversion at high sampling rates. We therefore focus on single carrier modulation and symbol rate sampling for the frequency-selective channel considered in this study.

In this paper, we explore *spatial oversampling* as a means of handling the dispersion caused by misalignments while maintaining symbol rate sampling. Since the overall area of the receive array including the original set of receive elements

is approximately equal to $147^2\lambda^2$ to satisfy the required spatial degrees of freedom, additional receive elements (beyond the number of transmitted streams) can be easily integrated into the receive array within the available form factor. In addition, we introduce the concept of an adaptive time window at each receive element, which accounts for the relative delays of the transmitted symbols at each receive antenna due to the geometric misalignment to align the received signals so as to reduce the required complexity of space-time equalization. We show that linear space-time equalizers of reasonable complexity, employing a suitable combination of spatial oversampling and adaptive time windowing, eliminate the error floors due to geometric misalignment that are incurred by conventional symmetric architectures in which the number of receive elements equals the number of spatially multiplexed streams.

Related work: The mmWave LoS MIMO links have been successfully deployed in industry (e.g., [8]), but we are interested in enabling large-scale deployments that do not require skilled installation, where misalignment would be a routine occurrence. There is a growing literature on the impact of such misalignments on LoS MIMO, but to the best of our knowledge, our proposed combination of spatial oversampling and adaptive time windowing has not been considered previously. In [9], a number of training-based and blind equalization algorithms are analyzed for 2×2 single-polarized and 4×4 dual-polarized LoS MIMO systems. Simulations performed at a carrier frequency of 19 GHz and symbol rate of 50 MHz show the need for complex receiver structures to handle frequency selectivity (e.g., time windows of more than 40 symbols in a space-time equalizer). The channel models and equalizers considered are more complex than ours. In [10], the authors propose a sequential channel equalization method for LoS MIMO in which the channel is factorized into a product of three matrices with the middle one dominated by an inverse discrete Fourier transform (DFT) matrix and the equalization is performed in a reverse order of factorization. However, symbol level dispersion is not modeled, unlike our setting, where pushing to large bandwidths of 10-20 GHz implies that even small misalignments lead to multi-symbol delay spread. Prior work involving our research group on the impact of geometric misalignments on LoS MIMO includes [5], [11]. In [5], an analog architecture with programmable sub-symbol delays is explored to alleviate the impact of differential delays across the receive array for a given transmitted stream. Spatial oversampling eliminates the need for such sub-symbol delays, as shown in [11], which is the approach closest to ours. However, the model in [11] employed random delays at each receive antenna, whereas the present paper introduces a more realistic delay spread model based on the specific system geometry corresponding to the misalignment angles and array size. We are able to exploit this more realistic model to introduce an adaptive windowing scheme that substantially reduces complexity relative to the generic scheme considered in [11]. We also provide detailed insight into the signal space considerations related to avoiding error floors with linear equalization, illuminating the tradeoff between the number of additional receive antennas and the temporal window used for equalization.

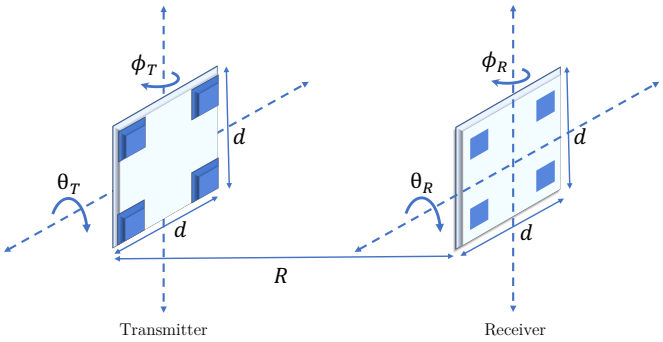

Fig. 1. Geometric misalignment configuration for the 4×4 LoS MIMO system

II. System Model

We consider a LoS MIMO system at $f_c = 130$ GHz with N_{TX} transmit and N_{RX} receive antennas at a link distance of R. Our running example, as shown in Fig. 1, assumes $N_{\text{TX}} = 4$ transmitters placed at the four corners of a $d = 34$ cm sided square aperture separated by $R = 100$ m from the $N_{\text{RX}} \geq 4$-element receiver of the same aperture. Four independent QPSK streams are transmitted from the four transmit antennas and linear MIMO reception techniques are employed at the receiver. The per-stream symbol rate is $B = 20$ GBd, corresponding to a symbol duration of $T_s = 50$ ps. The impulse response of the channel between transmitter n and receiver m is characterized by

$$h_{mn}(t) = \delta(t - \tau_{mn}). \tag{2}$$

Here, τ_{mn} is the delay parameter,

$$\tau_{mn} = \frac{R_{mn}}{c} + t^{\text{off}}_{\text{rx},m} - t^{\text{off}}_{\text{tx},n} \tag{3}$$

where R_{mn} is the distance between transmitter n and receiver m, c is the speed of light, and $t^{\text{off}}_{\text{tx},n}$ and $t^{\text{off}}_{\text{rx},m}$ are the (symbol-level) time reference offsets of transmitter n and receiver m, respectively. We partition the delay as $\tau_{mn} = \bar{\tau}_{mn} + \tilde{\tau}_{mn}$ where

$$\bar{\tau}_{mn} = [\tau_{mn}/T_s], \quad \tilde{\tau}_{mn} = \tau_{mn} - \bar{\tau}_{mn},$$

with $[\cdot]$ representing the rounding function. The QPSK data streams are modulated onto a raised cosine pulse train with roll-off factor of 0.25. Imperfect ADC sampling times causes the energy of each symbol to be spread out in time domain over multiple samples. For modeling the pulse spread, we consider a window of $L_P = 5$ samples for each pulse, which contains 99% of the pulse energy. The discretized signal at the ADC output of receiver m at time k is therefore described by,

$$y_m[k] = \sum_{n=1}^{N_{\text{TX}}} \sum_{l=-2}^{2} e^{-j2\pi f_c \tau_{mn}} s_n[k - \bar{\tau}_{mn} + l]\, p(\tilde{\tau}_{mn} - l) + w_n[k] \tag{4}$$

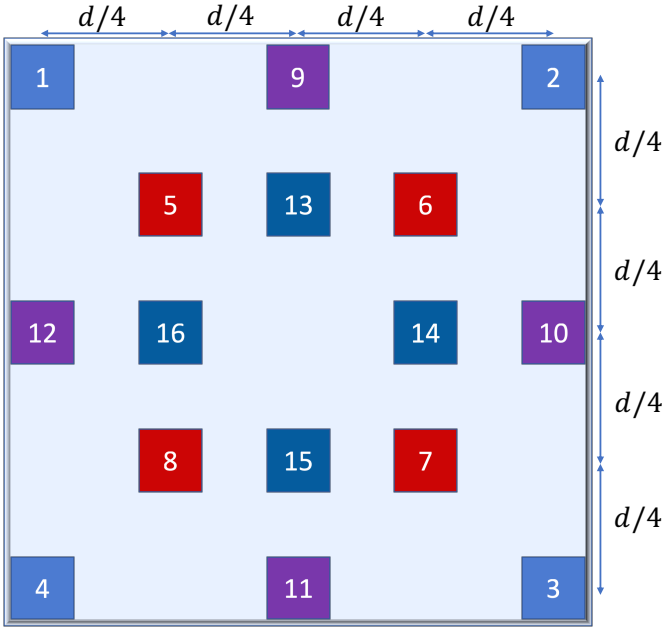

Fig. 2. $2\times$, $3\times$ and $4\times$ spatial oversampling within the same form factor

where $s_n[k]$ denotes the unit-amplitude QPSK symbol transmitted from antenna n at discrete time k ($|s_n[k]| = 1$), $w_n[k] \sim \mathcal{CN}(0, \sigma^2)$ are the iid additive complex Gaussian noise terms, and $p(t)$ is the raised cosine pulse function evaluated at time offset t.

When the antennas are oriented perfectly (facing each other), the path length differences between transmitter-receiver pairs is small, resulting in sub-symbol-period delays. However, even slight tilting of either platform can cause multiple-symbol delays across the aperture, necessitating space-time equalization for accurate decoding. We denote by θ_{T} and ϕ_{T} the elevation and azimuth rotation of the transmit array, and with θ_{R} and ϕ_{R} that of the receive array, as shown in Fig. 1. We consider rotations drawn randomly within the range of [-7.5,7.5] degrees for each of these parameters, resulting in up to 6-symbol delay offsets across the receive aperture.

Spatial oversampling: In order to facilitate equalization without increasing the ADC sampling rate beyond the signaling bandwidth, we rely on spatial oversampling. Increasing the number of receivers provides the necessary dimensions for effective interference suppression. The number of receivers considered in our system varies between 4 and 16, corresponding to a spatial oversampling factor of 1 (no oversampling) to 4. Fig. 2 shows the placement of receive antennas on the aperture. In order to attain sufficient link budget, each "receiver" may be realized as a fixed beam directive antenna or as a sub-wavelength spaced subarray performing electronic beamsteering (e.g., using RF beamforming) towards the transmitter.

Motivation for adaptive windowing: For the range of misalignments considered in our numerical examples, aggregating the effect of temporal pulse spread (due to off-peak sampling) and delay variation (due to platform tilt), the maximum spread

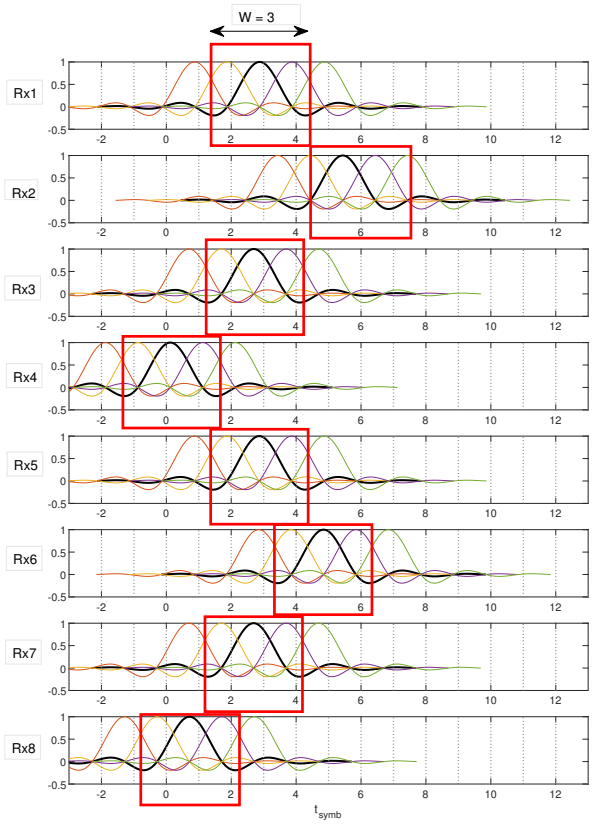

Fig. 3. Adaptive window, $W = 3$ described across $N_{RX} = 8$ receivers

in terms of samples for any given symbol across the receive array is at most equal to $t_{\text{spread}} = 5 + 6 = 11$. A naive space-time equalizer that employs a fixed window of time domain samples across all receive elements to make a decision on a given symbol would therefore need to employ a time window of 11 samples, leading to excessive complexity as we scale the number of receive elements. As we discuss in the next section, adaptive windowing together with spatial oversampling sidesteps this difficulty.

III. Adaptive Windowing

In this section, we introduce our adaptively-windowed space-time equalizer designed for the imperfectly aligned LoS MIMO systems. We explain our proposed framework via an example. Consider a 4×8 LoS MIMO system (i.e., spatial oversampling factor of 2), and consider a randomly generated misalignment between the transmit and receive arrays: $\theta_{\mathrm{T}} = 3.67°$, $\phi_{\mathrm{T}} = -4.30°$, $\theta_{\mathrm{R}} = 6.36°$, and $\phi_{\mathrm{R}} = 7.19°$. Consider demodulation of a "desired symbol" $x_1[k]$ transmitted from transmit antenna 1. Due to the different distances between transmit antenna 1 and the receive antennas, the time of arrival of the desired symbol at each receiver is different (see the black-colored pulses in Figure 3). The fainter pulses shown are the receive responses corresponding to past and future symbols emitted by transmit antenna 1. The integer values on x-axis of Figure 3 represents the sampling points of ADC at each receive antenna.

As seen in Figure 3, the considered misalignment causes up to 5-symbol delay offsets across the receive aperture. The peak response of the desired symbol $x_1[k]$ corresponds to a different time index at each receive antenna. The receiver can therefore adapt the window of samples employed at each antenna to align with the peak response from $x_1[k]$ at the antenna. Figure 3 illustrates a time window of size $W = 3$ at each receive antenna. Note that the time window at each receive antenna can, in principle, we adapted for each pair of transmit and receive elements, but we consider a fixed window size of W for simplicity. We employ a simple strategy: choose the window size W so as to capture "enough" of the energy of the desired symbol, and make sure that the resulting space-time equalizer of length WN_{RX} provides a large enough "signal space" dimension that linear interference suppression suffices for handling intersymbol interference (ISI) due to past and future symbols from the transmit antenna emitting the desired symbol, and the impact of cross-stream interference (CSI) due to symbols emitted by the other transmit antennas. The particular choice of $W = 3$ suffices to capture about 95% of the energy of the desired symbol for the raised cosine pulse considered. However, we might choose a larger window if the number of receive antennas is small, or a smaller window if the number of receive antennas is large, in order to trade off complexity against the twin goals of capturing enough energy from the desired symbol and providing sufficiently high signal space dimension.

Since the channel state information is available at the receiver, the receiver knows where they are and can employ an adaptive windowing approach in which the ADC output signals having the maximum contribution from $x_1[k]$ are aligned in time before the equalization is performed. By considering the aligned outputs at each receive antenna and a window of size W, $W\,N_{\text{RX}}$ output samples can be used to demodulate the desired symbol. The size of space-time equalization window can be chosen to get enough degrees of freedom and capture most of the desired signal energy. Also, W can be adaptively set and can vary on a transmit-receive pair basis. However, we consider the same window size for all transmit-receive pairs and leave the consideration of different window size for each transmit-receive pair as a future work.

Due to the different path length between each transmit-receive pairs and timing offsets at each transmit and receive antennas, the received symbols cannot be sampled at their peaks. Those imperfect sampling times causes the energy of each symbol to be spread out in time domain over multiple samples and the inter-symbol interference (ISI) occurs. For example, when we consider the received output of receive antenna 4 at time k, we obtain that the output has contribution from other previous and next symbols in the sequence as well as the main contribution from the desired symbol at time k, as shown in Figure 3.

In order to count the number of ISI and CSI symbols falling into the space-time window selected to demodulate a given desired symbol, let us assume that the modulating pulse for a symbol spans L_P samples (e.g., we may set $L_P = 5$ for our raised cosine pulse). For a time window of size W, a spread of $L = L_P + W - 1$ symbols from each antenna stream have non-negligible contribution to the samples in the observation window. Since we choose the window at each receive antenna to align around the peak response to the desired symbol transmitted from transmit antenna 1, the *same* set of ISI and CSI symbols fall into the chosen window for all receivers. Thus, the overall number of ISI symbols falling in the space-time window due to ISI is 6. Given W and L_P, the number of ISI symbols falling into the chosen window is $L - 1 = L_P + W - 2$. The number of CSI symbols falling into the window is $L(N_{\text{TX}} - 1)$, so that the total number of interfering symbols falling into the space-time window used to demodulate a desired symbol is $LN_{\text{TX}} - 1$. For $L_P = 5$ and $W = 3$, we have $L = L_P + W - 1 = 7$. The number of ISI symbols is $L - 1 = 6$, the number of CSI symbols is $L(N_{\text{TX}} - 1) = 21$, so that the total number of interfering symbols is 27. The vector response to each such interfering symbol within the space-time window is called an interference vector, while the vector response to the desired symbol is called the desired signal vector. The goal of linear space-time equalization, of course, is to suppress the interference vectors without incurring excessive noise enhancement. The dimension of the signal space in which we are operating is the length of the space-time equalizer, $W N_{\text{RX}}$.

We can concisely represent the preceding model by defining the channel H_s that produces the windowed observation vector for a desired symbol from stream s:

$$\begin{aligned}(\mathbf{y}_s)_{N_{\text{RX}}W\times 1} &= (\mathbf{H}_s)_{N_{\text{RX}}W\times N_{\text{TX}}L}\,(\mathbf{x}_s)_{N_{\text{TX}}L\times 1} \\ &= [\mathbf{h}_{s,1} \quad \mathbf{H}_{s,\text{ISI}} \quad \mathbf{H}_{s,\text{CSI}}] \begin{bmatrix} x_1 \\ \mathbf{x}_{\text{ISI}} \\ \mathbf{x}_{\text{CSI}} \end{bmatrix}, \quad (5)\end{aligned}$$

where $\mathbf{h}_{s,1}$ is the $N_{\text{RX}}W \times 1$ response of the desired symbol x_1 on the window, $\mathbf{H}_{s,\text{ISI}}$ is the $N_{\text{RX}}W \times (L-1)$ channel response of the $L-1$ ISI terms $\mathbf{x}_{\text{ISI}}$, and $\mathbf{H}_{s,\text{CSI}}$ is the $N_{\text{RX}}W \times (N_{\text{TX}}-1)L$ channel response of the $L-1$ CSI terms $\mathbf{x}_{\text{CSI}}$ on the observation window.

We consider linear Minimum Mean Squared Error (MMSE) equalization, which tends to the linear zero-forcing equalizer at high SNR, assuming that that the zero-forcing equalizer exists. If the zero-forcing equalizer does not exist, we expect to see error floors at high SNR due to residual interference. We therefore wish to operate in regimes in which the zero-forcing equalizer, which projects the received vector in the window along the direction of the desired vector orthogonal to the subspace spanned by the interference vectors, is likely to exist. Assuming that the interference vectors are linearly independent, a necessary condition (which is often sufficient) is that the dimension of the signal space is higher than the number of interference vectors. Therefore, by counting the number of interference vectors and comparing it with the length of the space-time equalizer, we obtain simple design rules of thumb regarding whether linear interference suppression can be expected to work well.

TABLE I
NUMBER OF INTERFERENCE VECTORS AND THE DIMENSION OF THE SIGNAL SPACE FOR DIFFERENT W WHEN $L_P = 5$ PER STREAM

W	Interference Vectors	Dimension of Signal Space				
		$N_{\mathbf{RX}} = 4$	$N_{\mathbf{RX}} = 6$	$N_{\mathbf{RX}} = 8$	$N_{\mathbf{RX}} = 12$	$N_{\mathbf{RX}} = 16$
1	19	4	6	8	12	16
3	27	12	18	24	36	48
5	35	20	30	40	60	80

In Table I, we provide the number of interference vectors and the corresponding dimension of the signal space based on different W values for the scenarios with a spatial oversampling factor of 1 to 4. From Table I, we obtain that the dimension of the signal space is less than the number of interference vectors for the 4×4 LoS system with no oversampling even if we consider different sizes for windowing (i.e., $W \in \{1, 3, 5\}$). Thus, linear space-time equalization is expected to perform poorly without spatial oversampling. For the 4×8 system with a window of size $W = 5$, we observe that the signal space dimension clearly exceeds the number of interfering vectors, implying that the LMMSE receiver is expected to perform well. It is important to note that for some cases in which the signal space dimension is less than the number of interferers, the LMMSE receiver may still perform well since some interference vectors are relatively weak, and residual interference due to the inability to completely suppress them is too small to lead to discernible error floors at the SNRs of interest.

LMMSE Receiver: The LMMSE receiver is calculated separately for each stream s based on that stream's adapted window and the ISI/interference terms that fall inside that window. Let us define the LN_{TX}-element set, Γ_s, containing indices of all the transmit symbols that fall into the space-time window used for decoding stream s. The extended channel model for stream s is thus represented by the $WN_{\text{RX}} \times LN_{\text{TX}}$ matrix $\mathbf{H}_s$, which is obtained by vectorizing the convolutional channel model in (4). For ease of exposition, we assume the first input dimension of H_s represents the desired symbol. Then, the $WN_{\text{RX}} \times 1$ LMMSE equalizer for stream s is given by

$$\mathbf{c}_s = (\mathbf{H}_s \mathbf{H}_s^{\mathbf{H}} + \sigma^2 \mathbf{I}_{WN_{\text{RX}}})^{-1} \mathbf{H}_s \boldsymbol{\delta}_1 \tag{6}$$

where $\boldsymbol{\delta}_1$ is a $|\Gamma_s|$-length vector whose value is 1 in the first entry and 0 everywhere else, effectively extracting the first column of the LMMSE estimator which corresponds to its output for the desired symbol. Then, the estimate for the desired transmitted input symbol of stream s is given by

$$\hat{x}_s = \mathbf{c}_s^{\mathbf{H}} \mathbf{y}_s. \tag{7}$$

where $\mathbf{y}_s$ is the vectorized representation of the received signal window for stream s. In our framework, N_{TX} such LMMSE receivers are computed, one for each of the transmitted data streams.

IV. SIMULATION RESULTS

In this section we evaluate the performance of our proposed framework for adaptively windowed space-time equalization in LMMSE MIMO reception with different window sizes and varying levels of spatial oversampling. We consider two performance metrics for our comparisons: (1) average per-stream bit error rate (BER), and (2) ratio of SINR to nominal (ideal) beamformed SNR. The nominal beamformed SNR is equal to

$$\text{SNR}_{\text{bf}} = \frac{N_{\text{RX}}}{\sigma^2}$$

which, with our assumption of unit amplitude channel gains and transmitted symbols, is a factor of N_{RX} higher than the SISO SNR. The SINR of stream s is evaluated based on our extended channel model and LMMSE receiver as

$$\text{SINR}_s = \frac{|\mathbf{c}_s^H \mathbf{H}_s \boldsymbol{\delta}_1|^2}{\sum_{\substack{i \in \Gamma_s \\ i \neq 1}} |\mathbf{c}_s^H \mathbf{H}_s \boldsymbol{\delta}_i|^2 + \sigma^2 |\mathbf{c}_s^H \mathbf{c}_s|^2} \tag{8}$$

where $\boldsymbol{\delta}_i$ is a $|\Gamma_s|$-long input vector with 1 on index i and zeros everywhere else. Note that, by our convention, index 1 corresponds to the desired symbol/signal vector of stream s falling into the adaptive receive window for that stream.

We model the nominal system described in Section II and average our results over 10^3 realizations, each with random horizontal and vertical shifts at the transmitter and receiver, drawn uniformly from $[-7.5°, 7.5°]$. Our analysis predicts that with insufficient spatial oversampling or window size, our system lacks the dimensionality required for full suppression of all interference vectors causing high-SNR BER floors.

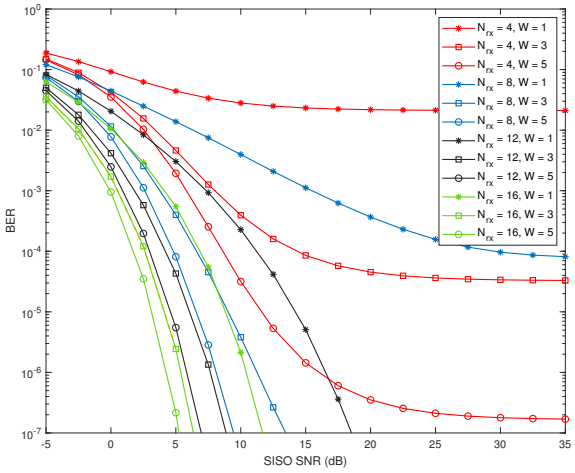

Fig. 4. Bit error rate versus SISO SNR for different values of N_{RX} and W.

Fig. 4 shows BER curves for different oversampling rates corresponding to $N_{\text{RX}} = 4$, 8, 12 and 16, and window sizes $W = 1$, 3, 5. As predicted, without spatial oversampling (i.e., $N_{\text{RX}} = 4$), there are BER floors even for larger window sizes. With spatial oversampling, however, error floors are circumvented even with relatively small window sizes, and as we increase the spatial oversampling factor, the minimum required window size for avoiding an interference bottleneck reduces. The observations of Fig. 4 are, for the most part, in keeping with the observation/interferer counting argument

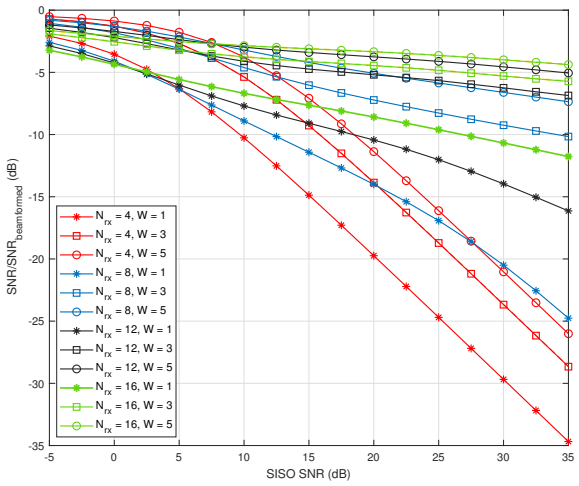

Fig. 5. SINR to beamformed SNR ratio versus SISO SNR for different values of N_{RX} and W

summarized in Table I, although the BER floor is not clearly visible for $N_{\mathrm{RX}} = 8, W = 3$. In order to better understand this slight disparity, we note that the 3 extra interferers counted in Table I are at the peripheries of the observation window and therefore severely attenuated by the raised cosine pulse. The LMMSE receiver therefore does not need to "expend signal space dimension" for suppressing these interference vectors. The BER floor due to the residual interference is too low to be captured by the BER plots, but the SINR to SNR gap can be more informative.

Fig. 5 shows the SINR to beamformed SNR ratio for the different cases. When full interference suppression (zero forcing) is not possible due to lack of dimensionality, this gap grows arbitrarily large as $\mathrm{SNR}_{\mathrm{bf}} \to \infty$. With sufficient dimensionality, on the other hand, the gap merges to a constant loss that results from the noise enhancement of the zero-forcing receiver. In this figure, the predictions of Table I are more clearly validated, as scenarios with a larger dimensionality deficit fall off faster as the system transitions from a noise-limited regime to an interference-limited regime.

V. Conclusion

The combination of spatial oversampling and adaptive time windowing has been shown to be a powerful approach for overcoming the intersymbol interference and cross-stream interference caused by geometric misalignments. A greedy strategy of selecting the space-time window for reception adaptively for each data stream so as to maximize desired signal strength is shown to be effective in reducing the computational complexity of linear space-time equalization. Simple signal space arguments comparing the number of interference vectors with the equalizer dimension provide accurate predictions of the level of spatial oversampling and temporal window size required for avoiding error floors at high SNR. For example, for 4 spatially multiplexed streams, a temporal window size of 3 suffices with 2X oversampling (8 receive antennas), and a window size of 1 suffices with 4X oversampling (16 receive antennas). Simulation results corroborate such analytical design guidelines.

With advances in mmWave RF design and packaging, it is becoming possible to realize one RF chain per antenna [12], with flexible disposition of antennas across the available aperture. The spatial oversampling enabled by such trends has been shown in prior work to improve robustness to impairments such as low ADC precision, nonlinearities, and phase noise. In future work, we hope to evaluate the potential of spatial oversampling in tackling the compounded effects of such phenomena, and investigate the extent to which spatial oversampling allows for relaxation of per-antenna specifications and simplification of equalization and signal processing in general. While transmit precoding was not considered in the present paper, the combination of transmit precoding with receive space-time equalization is an important topic for future research aimed at reducing complexity and power consumption in mmWave systems.

References

[1] I. Sarris and A. R. Nix, "Design and performance assessment of high-capacity MIMO architectures in the presence of a line-of-sight component," *IEEE Transactions on Vehicular Technology*, vol. 56, no. 4, pp. 2194–2202, 2007.

[2] M. Sawaby, B. Grave, C. Jany, C. Chen, S. Kananian, P. Calascibetta, F. Gianesello, and A. Arbabian, "A fully integrated 32 Gbps 2x2 LoS MIMO wireless link with UWB analog processing for point-to-point backhaul applications," in *2020 IEEE Radio Frequency Integrated Circuits Symposium (RFIC)*, 2020, pp. 107–110.

[3] E. Torkildson, U. Madhow, and M. Rodwell, "Indoor millimeter wave MIMO: Feasibility and performance," *IEEE Transactions on Wireless Communications*, vol. 10, no. 12, pp. 4150–4160, Dec. 2011.

[4] F. Bohagen, P. Orten, and G. E. Oien, "Design of optimal high-rank line-of-sight MIMO channels," *IEEE Transactions on Wireless Communications*, vol. 6, no. 4, pp. 1420–1425, 2007.

[5] B. Mamandipoor, M. Sawaby, A. Arbabian, and U. Madhow, "Hardware-constrained signal processing for mm-Wave LoS MIMO," in *2015 49th Asilomar Conference on Signals, Systems and Computers*, 2015, pp. 1427–1431.

[6] F. Pancaldi, G. M. Vitetta, R. Kalbasi, N. Al-Dhahir, M. Uysal, and H. Mheidat, "Single-carrier frequency domain equalization," *IEEE Signal Processing Magazine*, vol. 25, no. 5, pp. 37–56, 2008.

[7] J. Treichler, I. Fijalkow, and C. Johnson, "Fractionally spaced equalizers," *IEEE Signal Processing Magazine*, vol. 13, no. 3, pp. 65–81, 1996.

[8] Ericsson Press Release, "Deutsche Telekom and Ericsson top 100Gbps over microwave link," May 2019. [Online]. Available: https://www.ericsson.com/en/press-releases/2019/5/deutsche-telekom-and-ericsson-top-100gbps-over-microwave-link

[9] T. Ingason, H. Liu, M. Coldrey, A. Wolfgang, and J. Hansryd, "Impact of frequency selective channels on a line-of-sight MIMO microwave radio link," in *2010 IEEE 71st Vehicular Technology Conference*, 2010, pp. 1–5.

[10] X. Song, D. Cvetkovski, W. Rave, E. Grass, and G. Fettweis, "Sequential channel equalization in strong line-of-sight MIMO communication," *IEEE Transactions on Wireless Communications*, vol. 18, no. 1, pp. 340–356, 2019.

[11] P. Raviteja and U. Madhow, "Spatially oversampled demultiplexing in mmWave LoS MIMO," in *IEEE 19th International Workshop on Signal Processing Advances in Wireless Communications (SPAWC)*, June 2018, pp. 1–5.

[12] S. Abu-Surra, W. Choi, S. Choi, E. Seok, D. Kim, N. Sharma, S. Advani, V. Loseu, K. Bae, I. Na, A. A. Farid, M. J. W. Rodwell, G. Xu, and J. C. Zhang, "End-to-end 140 Ghz wireless link demonstration with fully-digital beamformed system," in *2021 IEEE International Conference on Communications Workshops (ICC Workshops)*, 2021, pp. 1–6.